Lithium ion as growth-controlling agent of ZnO nanoparticles prepared by organometallic synthesis†

Arnaud Glaria,[a] Myrtil L. Kahn,*[a] Thierry Cardinal,[b] François Senocq,[c] Véronique Jubera[b] and Bruno Chaudret*[a]

ZnO nanoparticles were synthesized by adding solid Zn(c-C_6H_{11})$_2$ to a THF solution of the lithium (sodium) precursor and octylamine (OA) as stabilizer. The proportion of Li (Na) was varied from 1 to 10 mol% compared to Zn. Two different lithium precursors namely Li[N(CH$_3$)$_2$] (series 1) and Li[N(Si(CH$_3$)$_3$)$_2$] (series 2) and one sodium precursor namely Na[N(Si(CH$_3$)$_3$)$_2$] (series 3) were used. Interestingly, Li precursors induce a modification of the growth of the particles while, no effect is observed when Na precursors is used. Indeed, isotropic nanoparticles were obtained when Li precursors were used while nanorods were formed with Na precursor as already observed in the same experimental conditions without alkali-metal precursor. Observations by TEM show that as the Li/Zn molar ratio increases, the mean diameters of the nanoparticles vary from 3.7 ± 0.7 nm to 2.5 ± 0.4 nm, and from 4.3 ± 1.0 nm to 3.1 ± 0.8 nm for series 1 and series 2, respectively, while the length and the diameter of the nanorods are *ca.* 11 × 4 nm, for series 3. Interestingly, the consequence of the lithium induced size variation leads to a shift of the emission band in the visible range, from yellow to blue through white as a function of increasing concentration of lithium precursor. The intensity of this emission is strong enough to be clearly seen by the human eye.

1 Introduction

ZnO is a wide-band-gap semiconductor (3.37 eV at room temperature) that displays among others, interesting luminescence properties in the near UV and visible spectrum ranges.[1] A renewed interest for this material has resulted from the progress in the synthesis of nanostructures achieved in the past few years.[2–6] The near UV emission corresponds to the excitonic luminescence and is based on the direct recombination of electron–hole pairs, while the emission components in the visible domain are more complex. The yellow–green emission around 550–580 nm is generally attributed to oxygen vacancies leading to hole trapped states.[3,7–15] In addition, a few papers reported the existence of a blue luminescence, the origin of which is still subject to controversies.[16–19] For all the systems discussed here above, it has been shown that the optical properties depend on several factors, namely the particle size and size dispersity, the shape of the particles, and their surface state, which depends on the synthetic method. Thus, various synthetic methods have been investigated to control the morphology of ZnO nanomaterials: physical methods (vapor phase oxidation,[20] thermal vapor transport and condensation (TVTC)[3,21–23] or chemical vapor deposition (CVD)[1,19,24]) or chemical methods (precipitation,[9,17,25–28] sol–gel,[4,29–31] hydrothermal reaction,[2,32–34] or microemulsion.[35] Among the chemical approaches, some of them make use of ionic species which may play a role in the growth process of the particles.[4,6,10,15,17,25–29,31,36–40] However, only few papers attempt to clearly identify the possible role of these ionic species (either anionic or cationic) in the growth process of the nanoparticles.[28,29,37]

In previous works, we evidenced the interest of an organometallic synthesis based on the Zn(c-C_6H_{11})$_2$ complex for the preparation of ZnO nanoparticles of controlled size and shape.[41,42] This method takes advantage of the exothermic reaction of the organometallic precursor with water, the kinetics of which is well controlled by the ligand present in the reaction solution. Importantly, this method only leads to the formation of ZnO nanoparticles and cyclohexane. The latter being volatile is eliminated. Moreover, the versatility of this method may allow us to introduce ionic species in order to study their influence on the growth process.

We report in this paper the influence of the presence of lithium ions on the growth process of ZnO nanoparticles together with the specificity of lithium compared to sodium and the consequences for the photoluminescence properties of the resulting nanoparticles.

[a] Laboratoire de Chimie de Coordination, UPR8241 CNRS, 205 route de Narbonne, 31077 Toulouse Cedex, France. E-mail: kahn@lcc-toulouse.fr, chaudret@lcc-toulouse.fr
[b] Institut de Chimie de la Matière Condensée de Bordeaux, ICMCB-CNRS, Université Bordeaux 1, 87 Av. Dr Schweitzer, 33608 Pessac, France
[c] Centre Inter Universitaire de Recherche et d'Ingénierie des Matériaux, UMR CNRS 5085, ENSIACET, Université Paul Sabatier, 31062 Toulouse Cedex 04, France. E-mail: kahn@lcc-toulouse.fr, chaudret@lcc-toulouse.fr

† Electronic supplementary information (ESI) available: Fig. S1: TEM pictures of ZnO nanorods obtained in absence of Li or Na ion. Fig. S2: XPS measurement on ZnO nanoparticles prepared in presence of 10% of [Li(NMe$_2$)$_2$] showing the presence of Li ions after the washing of the sample with deionized water. See DOI: 10.1039/b715583b

2 Results

2.1 Synthesis

The synthesis of ZnO nanoparticles was carried out following a procedure similar to that previously reported for ZnO nanoparticles.[41,42] It consists in the addition of $Zn(c\text{-}C_6H_{11})_2$ solid to a THF solution containing the lithium (sodium) precursor and octylamine (OA) as stabilizer. The proportion of Li (Na) was varied from 1 to 10 mol% compared to Zn. The resulting solution was then exposed to air and moisture leading after hydrolysis and solvent evaporation upon a two week period to a white and luminescent powder. Two series of ZnO nanoparticles were synthesized in this way using two different lithium precursors namely $Li[N(CH_3)_2]$ (series 1) and $Li[N(Si(CH_3)_3)_2]$ (series 2). A third series was prepared in the presence of sodium ions using $Na[N(Si(CH_3)_3)_2]$ (series 3). No post-treatment (neither sintering, nor washing) was performed. The final product is a solid hybrid material composed of nanoparticles surrounded by organic ligands, which provide the solubility of the nanoparticles in all organic solvents.

2.2 TEM measurements

The size and shape of the nanoparticles were determined by TEM measurements. Fig. 1, Fig. 2 and Fig. 3 show TEM pictures for series 1, series 2 and series 3, respectively. Interestingly, we observe that the introduction of a Li precursor changes the shape of the resulting nanoparticles. Indeed, when ZnO nanoparticles are prepared in the presence of Li precursors (see Fig. 1 and Fig. 2) nanoparticles of isotropic shapes are obtained, while in the absence of Li ions (see Fig. S1, ESI†) or in the presence of sodium ions (see Fig. 3), nanorods are obtained. Moreover, the size of the nanoparticles decreases as the Li amount increases whatever the Li precursor, while the size of the nanorods remains similar whatever the Na amount.
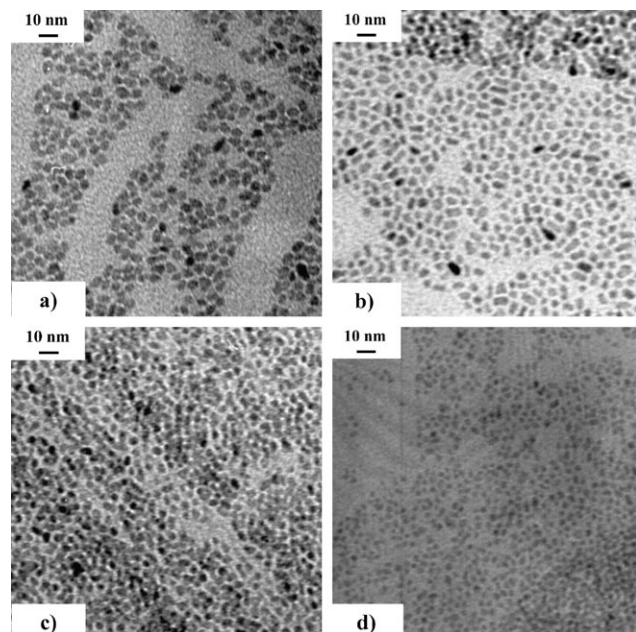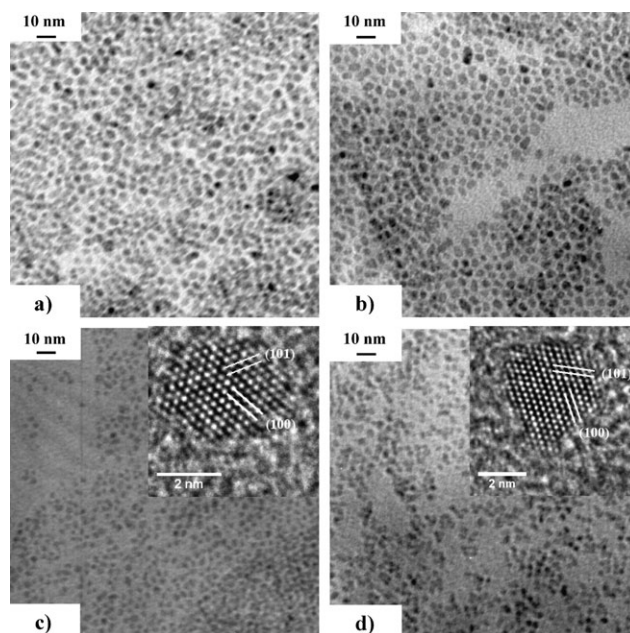

Fig. 2 TEM pictures of series 2 nanoparticles: (a) 1%, (b) 2%, (c) 5%, (d) 10% Li.

Indeed, as the Li/Zn molar ratio increases (from 1 to 10%), the mean diameters of the nanoparticles varies from 3.7 ± 0.7 nm to 2.5 ± 0.4 nm, and from 4.3 ± 1.0 nm to 3.1 ± 0.8 nm for series 1 and series 2, respectively, while the length and the diameter of the nanorods are in each case *ca.* 11×4 nm, for series 3. Table 1 reports the results obtained as a function of the experimental conditions.

HRTEM measurements have been performed on two samples containing, respectively 5 and 10 mol% Li in series 2. In both cases, monocrystalline nanoparticles have been
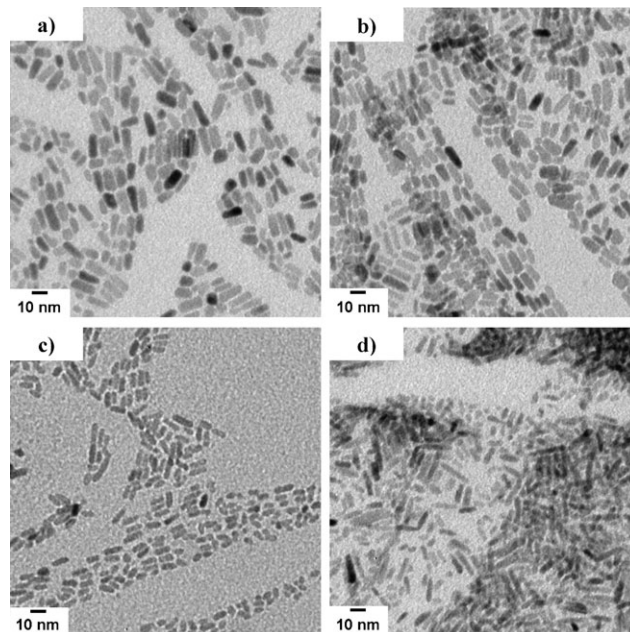

Fig. 1 TEM pictures of series 1 nanoparticles: (a) 1%, (b) 2%, (c) 5%, (d) 10% Li.

Fig. 3 TEM pictures of series 3 nanorods: (a) 1%, (b) 2%, (c) 5%, (d) 10% Na.

Table 1 Summary of the results obtained for the three series of samples. Size of the nanoparticles estimated from TEM and from XRD measurements, FWHM, bad-gap energy (E_g), and maximum of the emission band (λ_{max}) as a function of the percentage of alkali-metal ions introduced in the reaction solution

$\%^a$	TEM mean diameter^b/nm	$E_g{}^c$/nm	$\lambda_{max}(em)^d$/nm	FWHM $(hkl)^e/°$		Estimated dimension $(hkl)^f$/nm	
				(100)	(002)	(100)	(002)
Series 1: OA–Li[N(CH₃)₂]							
1	4.3 ± 1.0	356	582	1.58	1.63	4.8 ± 0.3	4.6 ± 0.3
2	3.8 ± 0.8	355	577	1.55	1.68	4.9 ± 0.3	4.5 ± 0.3
5	3.4 ± 0.6	346	541	1.76	2.57	4.3 ± 0.2	2.9 ± 0.1
10	3.1 ± 0.8	344	535	1.50	2.89	5.1 ± 0.4	2.6 ± 0.1
Series 2: OA–Li[N(Si(CH₃)₃)₂]							
1	3.7 ± 0.7	359	581	1.08	1.86	7.2 ± 0.8	4.1 ± 0.2
2	3.5 ± 0.5	354	574	1.96	2.46	3.9 ± 0.3	3.1 ± 0.2
5	2.6 ± 0.5	347	545	2.31	2.85	3.3 ± 0.2	2.6 ± 0.1
10	2.5 ± 0.4	345	534	3.20	2.86	2.4 ± 0.1	2.6 ± 0.1
Series 3: OA–Na[N(Si(CH₃)₃)₂]							
1	12.4 ± 2.8 × 4.9 ± 0.9	363	568	1.34	0.61	5.7 ± 0.4	13.4 ± 2.0
2	11.6 ± 2.9 × 4.5 ± 0.9	360	561	1.71	0.82	4.4 ± 0.2	9.6 ± 1.2
5	10.2 ± 2.0 × 3.4 ± 1.1	358	565	1.66	0.69	4.6 ± 0.3	11.6 ± 1.5
10	10.9 ± 2.4 × 3.2 ± 1.0	359	571	1.92	0.68	3.9 ± 0.3	11.8 ± 1.5

^{a} Percentage amount of lithium or sodium ions introduced in the reaction media. ^{b} The mean diameter is evaluated by fitting of the histogram with a Gaussian curve. The first value corresponds to the center of the peak whereas the second corresponds to twice the standard deviation of the Gaussian distribution or approximately 0.849 the width of the peak at half-height. ^{c} Inflexion point of the excitation spectra. ^{d} Maximum wavelength of the emission spectra. ^{e} Full width at half maximum; uncertainty ±0.10° ^{f} Dimension estimated through the Scherrer relation.

characterized (see inset of Fig. 2). These two samples were selected for their high Li content in order to search for some structural modifications induced by the insertion of Li ion in the ZnO lattice. However, whatever the sample, the hexagonal structure of ZnO has been observed.

2.3 X-ray measurements

X-Ray diffraction (XRD) measurements evidence the presence of the hexagonal zincite phase, space group $P6_3mc$ in all samples. Moreover, all diffractograms display additional peaks in the 2–30° 2θ range (not shown here) that can be ascribed to the octylamine ligand used during the synthesis as previously reported.[41] No crystalline hydroxide phase or lithium or sodium oxide phase is observed. Moreover, as the Li amount increases, a broadening of the ZnO diffraction peaks is observed whatever the Li precursor (see Fig. 4). The full width at half maximum (FWHM) for the (100) and (002) diffraction lines of the different series have been determined and are reported on Table 1. An estimation of the particle dimensions, using the Scherrer equation has been obtained at least in the perpendicular directions to the 100 and 002 planes. In series 1, an increase of the Li ratio leads to no significant change in the linewidth along the 100 perpendicular direction. However, along the c axis, an increase of the linewidth is detected which would correspond according to Scherrer equation to a size decrease of 4.6 ± 0.3 nm for 1% Li to 2.6 ± 0.1 nm for 10% Li. An interpretation of this observation could be the modification of the particle shape as a function of Li content from isotropic to flat pellets. The formation of ZnO nanopellets has previously been reported without any further explanation.[43] For series 2, the increase of Li ratio corresponds to an increase of the linewidths of both (100) and (002)

peaks. In this case, according to the Scherrer equation, this would correspond to an isotropic size decrease. In the case of series 3, the dimension calculated from the Scherrer equation from the (100) peak linewidth is in each case less than half that calculated for the (002) peak, therefore evidencing a nanorod shape. Overall, these XRD measurements confirm the influence of the Li content on the size variation of the particles as well as the difference of shapes between the nanoparticles prepared in the presence of Li and those prepared in the presence of Na.

2.4 Optical measurements

The optical properties of the three nanoparticle series were measured as colloidal solutions prepared by dissolving the solid samples in distilled THF. It is noteworthy that the colloidal solutions are stable in time and that no size or shape modifications were observed for several months. Particular care has been taken for the control of the colloidal solution concentration in order to keep the optical density below 0.25 near 320 nm to obtain an homogeneous absorption in the quartz cell for luminescence investigations and to avoid any modification of the excitation spectra due to the non-penetration of the incident light into the quartz cell. Absorption, excitation and emission spectra were measured for all samples. Fig. 5 shows the absorption spectra for the three series. All samples display a similar spectrum. They show a strong absorption between 300 and 350 nm followed by a sharp decrease. For some samples, a small decrease has been measured above 370 nm that could be related to light scattering of the solution. The absorption spectra are characteristic of nanosized particles of ZnO, the band gap of which is measured on the position of the inflection point. The curves obtained for
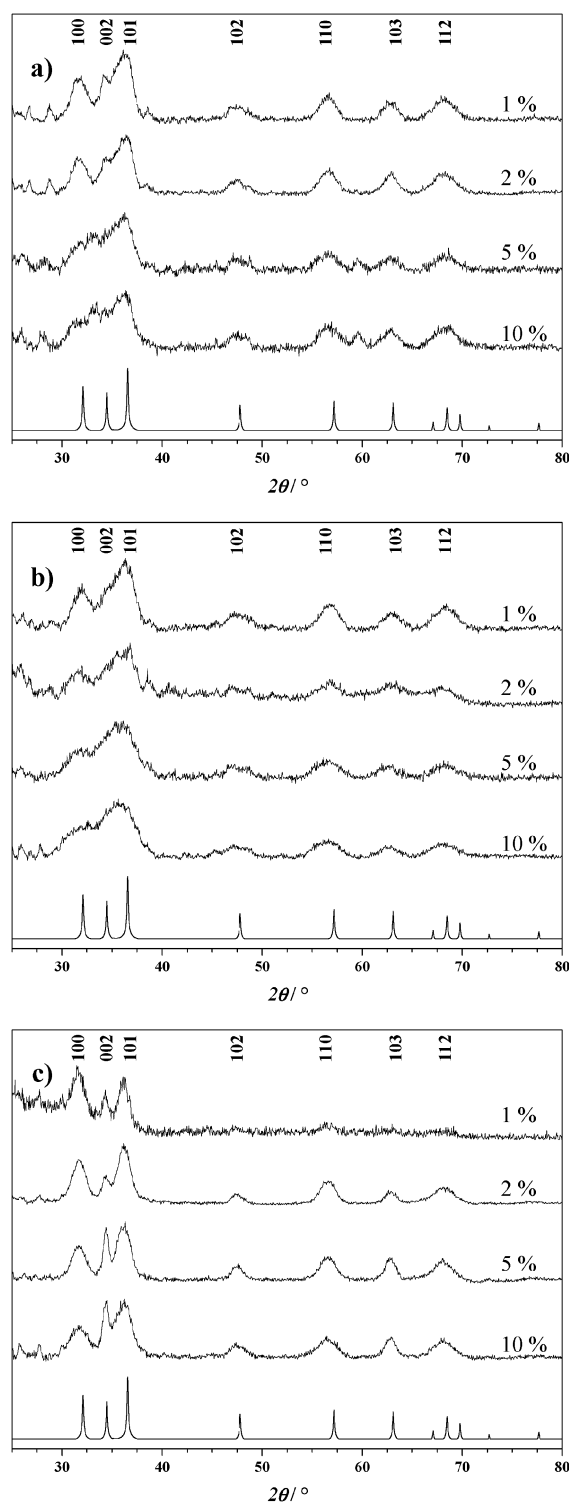
Fig. 4 Diffractograms of (a) series 1, (b) series 2, (c) series 3.

Fig. 5 Normalized absorption spectra for a Li/Zn molar ratio of 0.01 (▲), 0.02 (●), 0.05 (■) and 0.1 (—) of (a) series 1, (b) series 2, (c) series 3.

series 1 and series 2 show that the position of the inflection point depends on the Li content. In contrast, all samples of series 3 display similar absorption spectra, *i.e.* all curves possess a similar inflection point position. It is noteworthy that the absorption spectra of series 3 present a different signal to noise ratio compared to series 1 and series 2 because of the use of a different apparatus (see experimental part).
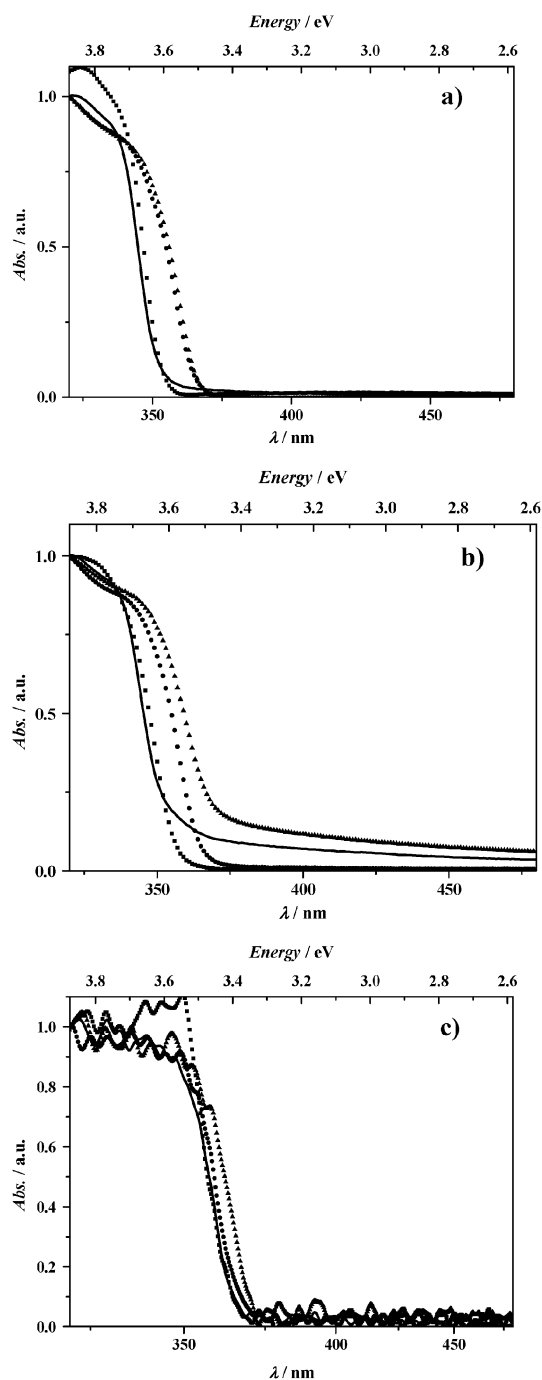
The luminescence properties of these samples were also investigated. Fig. 6 shows the normalized-emission and excitation spectra for the three series. One broad emission band is observed in the visible range for an excitation wavelength of 320 nm. The maximum of this emission band varies from 582 to 535 nm and from 581 to 534 nm for series 1 and series 2, respectively, while, for series 3, the maximum of the emission band remains constant at *ca.* 580 nm. Interestingly, the emission intensity is strong enough to be clearly seen by the human
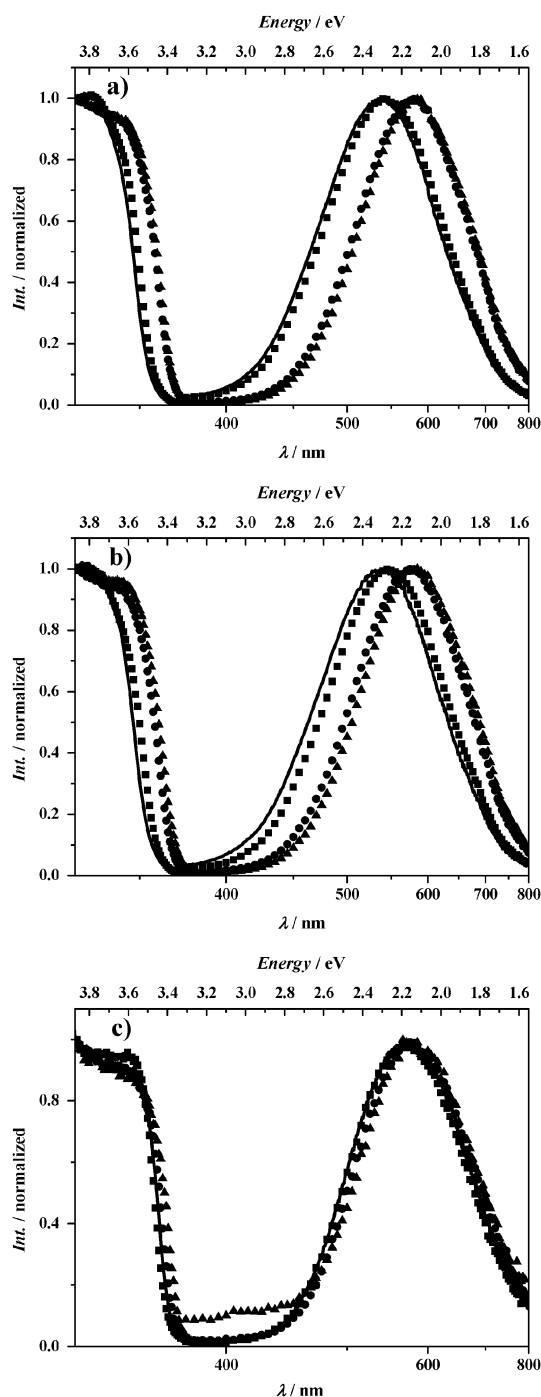
Fig. 6 Normalized excitation (left) and emission (right) spectra at room temperature for a Li/Zn molar ratio of 0.01 (▲), 0.02 (●), 0.05 (■) and 0.1 (—) (λ_{em} = 580 nm; λ_{exc} = 320 nm) of (a) series 1, (b) series 2, (c) series 3.

Fig. 7 Evolution of the emission at room temperature of the ZnO nanoparticles for series 2: (a) 1%, (b) 2%, (c) 5%, (d) 10%.

between the valence band and the conduction band which has previously been observed in the absorption spectra.

3 Discussion

We report in this paper the study of the influence of alkali-metal derivatives on the growth of ZnO nanoparticles through an organometallic approach allowing us to control precisely the composition of the reaction solution. The presence of organolithium precursors in the reaction medium changes the growth process of the nanoparticles. Thus, an isotropic shape is obtained in the presence of octylamine as ligand whatever the Li precursor, whereas ZnO nanorods are obtained in the same experimental conditions in the absence of a Li precursor or in the presence of a Na precursor. This effect may *a priori* result either only from the Li ions or from the generated amine, or from both, all the other parameters being kept constant. The hydrolysis of $Li[N(Si(CH_3)_3)_2]$ and $Li[N(CH_3)_2]$ lead in both cases to LiOH together with the amines $HN(Si(CH_3)_3)_2$ and $HN(CH_3)_2$, respectively. However, in the experimental conditions, $HN(Si(CH_3)_3)_2$ may remain in the reaction medium, while $HN(CH_3)_2$ is volatile and thus, is eliminated from the medium. Therefore $HN(CH_3)_2$ is unlikely to play any role in the growth process and we can assume that the Li ions are responsible for the different shapes of nanoparticles observed in the presence or not of Li precursors. In order to get more information on the localization of the Li ions in the ZnO nanoparticles, we tried to perform EELS measurements. EELS measurements necessitate high focalization of the electron beam and unfortunately, the energy of the electron beam leads to the vaporization of the Li ions preventing any observation. An alternative to the influence of Li in the shape modification might arise from the small amount of THF used to introduce the organolithium complex in the reaction media. However, we can assert that this small THF

eye as illustrated in Fig. 7. In this figure, the emitted light arise from the irradiation with a standard UV lamp (λ = 254 nm) of a drop of the colloidal solution deposited on a filter-paper used for the preparation of the TEM grid. Excitation spectra recorded for an emission wavelength of 580 nm present a strong absorption below 375 nm. Overall, all excitation spectra display a similar shape which is characteristic of an intrinsic absorption of the material. This corresponds to the transition
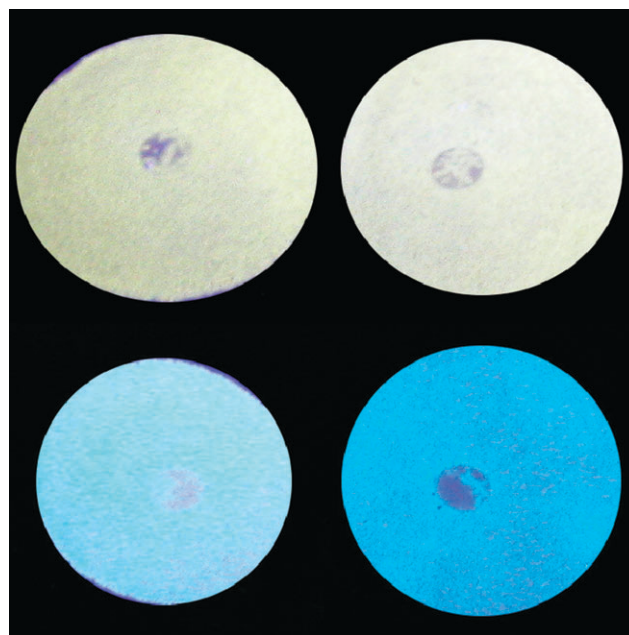
amount is not at the origin of the shape modification, because the same experimental conditions have been used to introduce the organosodium complex and, in this case, no shape modification has been observed.

An Li content increase from 1 to 10% corresponds to a *ca.* 30% decrease of the particle size whatever the Li precursor. The nanoparticle size is nevertheless slightly larger (0.6 nm on average) when $Li[N(CH_3)_2]$ is used. This may arise from the difference in the hydrolysis rate of the Li precursors pointing out the importance of the Li-precursor choice. In any case, the shape modification of the particles and the decrease of the particle size as the amount of Li increases results from the presence of the Li ions in the reaction solution. The Li ions may block the growth of the particles by deposition at the surface of the ZnO nanoparticles whatever their location (substitution of a Zn position, formation of an alloy phase or statistical deposition). Several papers report on the control of the size of ZnO nanoparticles using polymers[15,31,36,37,39,40] or ionic liquid[38] and LiOH. For example, Xiong *et al.* have reported a decrease of the particle size when the [LiOH]/[Zn] ratio varies form 1 to 3.5.[31,39,40] The authors have mentioned that at low LiOH concentration ([LiOH]/[Zn] = 1 or 1.4), the stabilization of the nanoparticles is ensured by the PEGME polymer and that at high LiOH concentration ([LiOH]/[Zn] = 3.4), the excess of LiOH can prevent the growth of the PEGME-stabilized ZnO particles. The same trend has been observed by Liu and co-workers using ionic liquids instead of polymer.[38] Abdullah *et al.* have also reported that the use of a high concentration of LiOH gives smaller PEGME-stabilized ZnO particles.[36,37] Moreover, these authors have reported that the remaining unreacted lithium hydroxide could be distributed around the ZnO particles as an amorphous layer preventing any agglomeration. Those results are in agreement with ours showing that the presence of Li ions in the reaction medium plays a crucial role on the size control. The concentration at which we observe the lithium effect is however much lower ([Li]/[Zn] ranges from 0.01 to 0.1) and, in our case, the stabilization of the colloidal solution is ensured by octylamine ligand. The effect of lithium ions on the particle growth is clear when considering the results obtained when the syntheses are performed in all the same conditions but using sodium instead of lithium. In these cases, we do not observe any shape and size modification. Nanorods of around 11 × 4.5 nm are constantly observed. Careful attention on the diameter of the rods allows observing that the diameter of the ZnO nanorods obtained in presence of 1 and 2% of Na precursor is close to 4.5 nm, while the diameter of the rods for 5 and 10% is close to 3.5 nm for a length remaining close to 11 nm (see Table 1). This variation is very small and we believe is not due to the presence of Na ions. Moreover, such a size variation has only a weak influence on the optical properties of series 3. The difference between the respective influences of Li and Na ions on the shape and size of the nanoparticles may arise from the values of their covalent radii, namely 1.23 and 1.54 Å for Li and Na atoms, respectively. These values have to be compared to 1.25 Å for Zn atom. Clearly, Li possesses a covalent radius that fits well with the value of Zn while the Na value is too large to allow the insertion of Na ions in the nanoparticles. We also wondered if the size variations and consequently the spectral changes may

be due to Ostwald ripening, as several papers reported such an observation.[4,6,25,26,28] An efficient way to access to this information is to perform absorption and emission spectra as a function of time. However, we never observed modifications of the absorption and emission spectra as a function of time, excluding therefore an evolution of the size of the nanoparticles.

The optical properties observed for series 1 and series 2 correspond to a modification of the band-gap as mentioned here above. This has to be related to the size reduction observed as the Li amount increases. Interestingly, the modification of the band-gap value is important when the Li amount varies from 1 to 5% but is less important from 5 to 10%. These results seem to indicate a saturation phenomenon that could be due to a saturation of lithium ions either in the particles or on their surface. For series 3, the absorption spectra are consistent with the TEM pictures showing no size modification as the Na amount varies.

Emission spectra of the three series present only one emission band in the visible range that corresponds to the oxygen-vacancies band (Fig. 6).[3,7–14] Two different behaviors can be distinguished. For series 1 and series 2, a blue shift of the emission band is observed from 580 to 540 nm when the Li amount increases from 1 to 10%, whereas no variation of the maximum of the emission band is observed when Na ion is used (series 3). These evolutions are in agreement with the results obtained for both the absorption and the excitation spectra. Indeed, these absorption spectra are characteristic of a mechanism involving the transition of the photogenerated electron from the valence band to the conduction band. These results are clearly related to the size of the nanoparticles (size variation for series 1 and 2 and no size variation for series 3). However, special attention to the emission spectra reveals some interesting features in the two ZnO nanoparticle series prepared in presence of Li precursor, namely series 1 and series 2. Despite the fact that the synthesis conditions are rigorously identical for series 1 and series 2 and the absence of post-treatments (neither heating, extraction, nor vacuum treatment) the maximum values of the emission band are similar for series 1 and series 2 at a given Li content even though the size of the particles are different. Conversely for the same size of particles but different Li contents, two different positions are observed for the maximum of the emission in the visible range when considering series 1 or series 2. These observations indicate that the population of defects at the origin of the luminescence could be different and have to be related to the difference of the Li precursor used for series 1 and series 2. These results suggest that the Li-containing-ZnO nanoparticles may, in fact, be constituted of a core of ZnO surrounded by a ZnO:Li layer, the thickness of which is directly related to the quantity of Li introduced during the synthesis and the hydrolysis rate of the Li-precursor. Different phases containing Li ions can be found in the literature: either $Li_xZn_yO_z$, Li_xO_y or $Li(OH)$.[44] However, in our samples, none of these phases has been observed by XRD measurements suggesting that the Li containing phase is either amorphous or too thin to diffract. ICP and XPS measurement were performed to prove the presence of the alkali-metal ions in the material after its washing using deionized water. Samples prepared in presence

of 10% of alkali-metal precursors were chosen since the detection of Li ions by XPS is difficult due to the very small cross section. In any case, around 1–3% of the alkali-metal ions were detected (see ESI,† Fig. S2). Such characterization on nanoparticles of this small size confirms the presence of the alkali-metal ions but does not allow to localize them. In any case, the characterization of the phase surrounding the ZnO core is difficult as previously reported by Noack and Eychmuller.[29] The observations that are in favor of the formation of a core–shell structure with a ZnO core surrounded by a Li containing ZnO phase are (i) the size variation observed when Li ions are introduced in the reaction media; (ii) the position of the emission band and its variation with the concentration of Li ions, and (iii) that none of the Li containing phase reported in the literature is luminescent. Consequently, the optical properties measured on these samples can only come from the ZnO phase. Such observations are in agreement with the growth process of the nanoparticles that we have discussed above.

4 Conclusion

In conclusion, we report in this paper the preparation of mixed ZnO/Li and ZnO/Na nanoparticles by co-hydrolysis of a zinc and a lithium (sodium) precursor as well as the important role of Li ions at the periphery of ZnO nanoparticles to control their size. This size control is surprising and may result from the different hydrolysis rates of the zinc and lithium precursors. Furthermore, the choice of the Li precursor is also a key point as its hydrolysis rate influences the incorporation rate of the Li ion in the ZnO nanoparticles. In contrast, the introduction of a sodium precursor in the reaction solution does not modify the size or shape of the resulting ZnO nanorods and therefore does not modify their luminescence. Interestingly, the presence of Li ions leads to a blue shift of the emission band of the ZnO nanoparticles. This blue shift is larger as the concentration of precursor increases and consequently as the size of the nanoparticles decreases. In this way, colloidal solutions and nanoparticles in the solid state are obtained which display a luminescence in the visible range from yellow to blue through white and which can be stored for several months without any modification of their optical properties. The emission intensity is strong enough to be clearly seen by the human eye and opens perspectives for the preparation of LEDs.

5 Experimental

5.1 Synthetic procedures

All reactions were performed under argon atmosphere using standard Schlenk tubes (14/19 opening) and vacuum-line techniques. The solvents used were dried (THF over Na/benzophenone, pentane over CaH_2) and freshly distilled prior to use. $Zn(c$-$C_6H_{11})_2$ was prepared as describe in the literature and was stored in the glove-box fridge.[45] $Li[N(CH_3)_2]$ was purchased from Aldrich and employed as received. $Li[N$-$(Si(CH_3)_3)_2]$ was prepared by adding one equivalent of n-BuLi dropwise (1.6 M in hexane, 18.8 mL, 30 mmol) to

$HN(Si(CH_3)_3)_2$ (6.4 mL, 30 mmol) under vigorous stirring in pentane at –78 °C. A white precipitate appeared and the mixture was then allowed to warm to room temperature. Finally, the volatiles were removed under vacuum, leading to the white product characterized by ^{1}H NMR in THF-d_8: CH_3 (s, –0.16 ppm) that can be compared to CH_3 (s, 0.08 ppm) of $HN(Si(CH_3)_3)_2$.

As a standard procedure, ZnO nanoparticles were obtained as follows. Both precursors and ligands were introduced under argon and left to react at room temperature for 17 h. The system was then exposed to ambient air and moisture by removing the stopper until the complete formation of the white product corresponding to the nanoparticles (typically for a period of 2 weeks). Practically, 3.7 ± 0.7 nm nanoparticles were obtained by addition of a THF solution of $Li[N$-$(Si(CH_3)_3)_2]$ (25 μL, 2.5 μmol) to a mixture of $Zn(c$-$C_6H_{11})_2$ (57.9 mg, 0.250 mmol) and one equivalent of octylamine (OA) (47.6 μL, 0.252 mmol). Increasing the volume of lithium-containing THF solution to 50, 125 and 250 μL, nanoparticles with a mean diameter of, respectively 3.5 ± 0.5, 2.6 ± 0.5, and 2.5 ± 0.4 nm are obtained. Using 25, 50, 125 or 250 μL of $Li[N(CH_3)_2]$ (0.1 M) instead of $Li[N(Si(CH_3)_3)_2]$ produces nanoparticles of 4.3 ± 1.0, 3.8 ± 0.8, 3.4 ± 0.6, and 3.1 ± 0.8 nm, respectively. The exchange of Li for Na leads to the formation of nanorods of around 11×4 nm whatever the quantity of Na introduced in the reaction media, respectively 25, 50, 125 or 250 μL of a THF solution of $Na[N(Si(CH_3)_3)_2]$ (0.1 M) precursor.

5.2 TEM experiments

The TEM specimens were prepared by slow evaporation of droplets of colloidal solution of the different samples deposited on carbon-supported copper grids. The experiments were performed on a JEOL200CX operating at 200 kV.

The size distribution was determined manually by an analysis of low-magnification TEM images. In this procedure, the different particles were visually identified according to an upper and lower intensity threshold and then counted and measured. Histograms of the size distribution include the measurement of at least two hundred particles and were reproduced in different regions of the samples. The size distribution was evaluated by fitting the histogram with a Gaussian curve. The size of the nanoparticles is given in the following form: $x \pm y$ nm. The first value corresponds to the center of the peak whereas the second one corresponds to twice the standard deviation of the Gaussian distribution which corresponds to approximately 0.849 the width of the peak at half-height.

5.3 X-Ray diffraction

The powder-diffraction patterns were obtained using a SEIFERT XRD 3000 TT X-ray diffractometer with Cu-Kα radiation, fitted with a diffracted-beam graphite monochromator. The data were collected in the θ/θ configuration.

5.4 Optical measurements

Absorption spectra were recorded using a double beam spectrophotometer (CARY 5000 UV-VIS-NIR) between 200 and

800 nm for series 1 and series 2, while a homemade absorption spectrometer was used for series 3. The emission spectra were recorded using a spectrofluorimeter (Edinburgh Instruments FL 900 CDT) with a PM Hamamatsu R955 for visible detection. A Xe lamp was used as excitation source.

5.5 XPS measurements

XPS spectra were recorded using an SSI M-Probe spectrometer at room temperature. A monochromatic Al-Kα X-ray (1486.6 eV) was used for the excitation. The analysis chamber pressure was of 5×10^{-9} mbar. Survey spectra were recorded at constant pass energy of 150 eV for quantitative analyses and 50 eV for high-resolution analysis. A 5 eV flood gun was used in order to prevent charge effects. Experimental and theoretical bands were fitted (80% Gaussian and 20% Lorentzian) using a non-linear baseline with a least-square algorithm. Quantitative analyses were calculated using Scofield factors[46] and binding energies were determined using the C 1s binding energy of C–C, C–H type carbon (284.6 eV) as the reference with an experimental error of ±0.2 eV.

Acknowledgements

References

1 M. H. Huang, S. Mao, H. Feick, H. Yan, Y. Wu, H. Kind, E. Weber, R. Russo and P. Yang, *Science*, 2001, **292**, 1897–1899.
2 A. B. Djurisic, W. C. H. Choy, V. A. L. Roy, Y. H. Leung, C. Y. Kwong, K. W. Cheah, T. K. G. Rao, W. K. Chan, H. F. Lui and C. Surya, *Adv. Funct. Mater.*, 2004, **14**, 856–864.
3 B. H. Juarez, P. D. Garcia, D. Golmayo, A. Blanco and C. Lopez, *Adv. Mater.*, 2005, **17**, 2761–2765.
4 C. Pacholski, A. Kornowski and H. Weller, *Angew. Chem., Int. Ed.*, 2002, **41**, 1188–1191.
5 L. Spanhel and M. A. Anderson, *J. Am. Chem. Soc.*, 1991, **113**, 2826–2833.
6 Z. R. Tian, J. A. Voigt, J. Liu, B. McKenzie, M. J. McDermott, M. A. Rodriguez, H. Konishi and H. Xu, *Nat. Mater.*, 2003, **2**, 821–826.
7 V. A. Fonoberov and A. A. Balandin, *Phys. Rev. B*, 2004, **70**, 195410.
8 Y. Gu, I. L. Kuskovsky, M. Yin, S. O'Brien and G. F. Neumark, *Appl. Phys. Lett.*, 2004, **85**, 3833–3835.
9 Ischenko, V. S. Polarz, D. Grote, V. Stavarache, K. Fink and M. Driess, *Adv. Funct. Mater.*, 2005, **15**, 1945–1954.
10 N. S. Norberg and D. R. Gamelin, *J. Phys. Chem. B*, 2005, **109**, 20810–20816.
11 A. van Dijken, J. Makkinje and A. Meijerink, *J. Lumin.*, 2001, **92**, 323–328.
12 A. van Dijken, E. A. Meulenkamp, D. Vanmaekelbergh and A. Meijerink, *J. Phys. Chem. B*, 2000, **104**, 1715–1723.
13 K. Vanheusden, W. L. Warren, C. H. Seager, D. R. Tallant, J. A. Voigt and B. E. Gnade, *J. Appl. Phys.*, 1996, **79**, 7983–7990.
14 Z. Wang, C. Lin, X. Liu, G. Li, Y. Luo, Z. Quan, H. Xiang and J. Lin, *J. Phys. Chem. B*, 2006, **110**, 9469–9476.
15 H.-M. Xiong, D.-P. Xie, X.-Y. Guan, Y.-J. Tan and Y.-Y. Xia, *J. Mater. Chem.*, 2007, **17**, 2490–2496.
16 M. L. Kahn, T. Cardinal, B. Bousquet, M. Monge, V. Jubera and B. Chaudret, *ChemPhysChem*, 2006, **7**, 2392–2397.
17 S. Monticone, R. Tufeu and A. V. Kanaev, *J. Phys. Chem. B*, 1998, **102**, 2854–2862.
18 H. Zeng, W. Cai, J. Hu, G. Duan, P. Liu and Y. Li, *Appl. Phys. Lett.*, 2006, **88**, 171910.
19 A. Zubiaga, J. A. García, F. Plazaola, F. Tuomisto, K. Saarinen, J. Zuñiga Pérez and V. Muñoz-Sanjosé, *J. Appl. Phys.*, 2006, **99**, 053516.
20 J. Q. Hu, Q. Li, N. B. Wong, C. S. Lee and S. T. Lee, *Chem. Mater.*, 2002, **14**, 1216–1219.
21 S. Chen, S. Liu, C. Shao, R. Mu, Y. Lu, J. Zhang, D. Shen and X. Fan, *Adv. Mater.*, 2005, **17**, 586–590.
22 H. J. Fan, W. Lee, R. Hauschild, M. Alexe, G. Le Rhun, R. Scholz, A. Dadgar, K. Nielsch, H. Kalt, A. Krost, M. Zacharias and U. Gosele, *Small*, 2006, **2**, 561–568.
23 Y. Zhang, L. Wang, X. Lui, Y. Yan, C. Chen and J. Zhu, *J. Phys. Chem. B*, 2005, **109**, 13091–13093.
24 X. Wang, J. Song, P. Li, J. H. Ryou, R. D. Dupuis, C. J. Summers and Z. L. Wang, *J. Am. Chem. Soc.*, 2005, **127**, 7920–7923.
25 Z. Hu, G. Oskam, R. L. Penn, N. Pesika and P. C. Searson, *J. Phys. Chem. B*, 2003, **107**, 3124–3130.
26 E. A. Meulenkamp, *J. Phys. Chem. B*, 1998, **102**, 5566–5572.
27 P. V. Radovanovic, N. S. Norberg, K. E. McNally and D. R. Gamelin, *J. Am. Chem. Soc.*, 2002, **124**, 15192–15193.
28 R. Viswanatha, H. Amenitsch and D. D. Sarma, *J. Am. Chem. Soc.*, 2007, **129**, 4470–4475.
29 V. Noack and A. Eychmuller, *Chem. Mater.*, 2002, **14**, 1411–1417.
30 S. C. Pillai, J. M. Kelly, D. E. McCormack, P. O'Brien and R. Ramesh, *J. Mater. Chem.*, 2003, **13**, 2586–2590.
31 H. M. Xiong, X. Zhao and J. S. Chen, *J. Phys. Chem. B*, 2001, **105**, 10169–10174.
32 S. Kar, A. Dev and S. Chaudhuri, *J. Phys. Chem. B*, 2006, **110**, 17848–17853.
33 M. Mo, J. C. Yu, L. Zhang and S.-K. A. Li, *Adv. Mater.*, 2005, **17**, 756–760.
34 Q. Tang, W. Zhou, J. Shen, W. Zhang, L. Kong and Y. Qian, *Chem. Commun.*, 2004, 712–713.
35 L. Guo, Y. L. Ji, H. Xu, P. Simon and Z. Wu, *J. Am. Chem. Soc.*, 2002, **124**, 14864–14865.
36 M. Abdullah, I. W. Lenggoro, K. Okuyama and F. G. Shi, *J. Phys. Chem. B*, 2003, **107**, 1957–1961.
37 M. Abdullah, T. Morimoto and K. Okuyama, *Adv. Funct. Mater.*, 2003, **13**, 800–804.
38 D.-P. Liu, G.-D. Li, Y. Su and J.-S. Chen, *Angew. Chem., Int. Ed.*, 2006, **45**, 7370–7373.
39 H.-M. Xiong, D.-P. Liu, Y.-Y. Xia and J.-S. Chen, *Chem. Mater.*, 2005, **17**, 3062–3064.
40 H.-M. Xiong, Z.-D. Wang, D.-P. Liu, J.-S. Chen, Y.-G. Wang and Y.-Y. Xia, *Adv. Funct. Mater.*, 2005, **15**, 1751–1756.
41 M. L. Kahn, M. Monge, V. Collière, F. Senocq, A. Maisonnat and B. Chaudret, *Adv. Funct. Mater.*, 2005, **15**, 458–468.
42 M. Monge, M. L. Kahn, A. Maisonnat and B. Chaudret, *Angew. Chem., Int. Ed.*, 2003, **42**, 5321–5324.
43 D. P. Cozzoli, L. M. Curri, A. Agostiano, G. Leo and M. Lomascolo, *J. Phys. Chem. B*, 2003, **107**, 4756–4762.
44 ICCD PDF 2, release 2006.
45 K. H. Thiele, S. Wilcke and M. Ehrhardt, *J. Organomet. Chem.*, 1968, **14**, 13–19.
46 J. H. Scofield, *J. Electron Spectrosc. Relat. Phenom.*, 1976, **8**, 129.